# Experiments on Hydrodynamic Stability of Laser-Driven Detonations in Nitrogen and Helium Gases

**Tomohisa Honda[1], Akira Kawaguchi[1], Yoshiki Hanta[1], Akio Susa[1], Shinichi Namba[1], Takuma Endo[1], Hiroyuki Shiraga[2], Keisuke Shigemori[2], and Mayuko Koga[2]**

[1]Department of Mechanical Systems Engineering, Hiroshima University,
1-4-1 Kagamiyama, Higashi-Hiroshima, Hiroshima 739-8527, Japan

[2]Institute of Laser Engineering, Osaka University,
2-6 Yamada-oka, Suita, Osaka 565-0871, Japan

## 1 Introduction

Detonation is originally a technical term in the research field of chemical combustion [1,2]. However, two other types of detonation are now known: laser-driven (LD) detonation [3-5] and nuclear-combustion-driven (NCD) detonation [6-8]. Their common feature is that shock waves and fluid-heating zones propagate together interactively, whose propagation speed is given by the Chapman-Jouguet (CJ) condition as

$$D_{\mathrm{CJ}} = \sqrt{2\left(\gamma_{\mathrm{CJ}}{}^2 - 1\right)\left(q_{\mathrm{react}} + q_{\mathrm{ext}}\right)} \qquad (1)$$

where $\gamma_{\mathrm{CJ}}$, $q_{\mathrm{react}}$, $q_{\mathrm{ext}}$ are respectively the specific-heat ratio at the rear surface, the heat of reaction per unit mass, and the added heat from external energy source per unit mass. In chemical-combustion-driven (CCD) and NCD detonations, $q_{\mathrm{react}} > 0$ and $q_{\mathrm{ext}} = 0$. However, $q_{\mathrm{react}} < 0$ and $q_{\mathrm{ext}} > 0$ in LD detonations. So far, CCD detonations have been extensively studied. It is well known that an actual detonation speed agrees well with the calculated $D_{\mathrm{CJ}}$, and also that an actual detonation front is not planar but composed of many micro explosions. On the other hand, details of LD and NCD detonations have hardly been known. They differ from a CCD detonation in that they contain hot plasmas. Because particles with long mean free path are produced in the hot plasma, the nature of LD and NCD detonations might be significantly affected by their transport.

When a sold plate placed in a gas is irradiated by laser with appropriate energy flux, a seed plasma is created on the surface of the solid plate, and an LD detonation propagates from the seed plasma toward the opposite direction to the drive laser as shown in Fig. 1. The one-dimensional structure of an LD detonation is schematically shown in Fig. 2. The drive laser starts to be absorbed in the shock-produced plasma. By the laser heating of

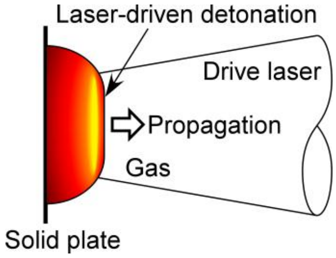


Fig. 1 Laser-driven detonation initiated on a solid plate.

the plasma, its ionization proceeds downstream. Because the laser-absorption coefficient due to inverse bremsstrahlung per unit length $\kappa$ is scaled as [9]

$$\kappa \propto \frac{z^2 n_e n_i}{T_e^{3/2}\sqrt{1-\left(n_e/n_{cr}\right)}} \qquad (2)$$

where $z$, $n_e$, $n_i$, $T_e$, $n_{cr}$ are, respectively, ionic charge state, electron density, ion density, electron temperature, and critical electron density for the laser, the laser heating becomes remarkable nonlinearly as the ionization proceeds. This is a simplified description of an LD detonation. The particles with long mean free path might induce significant preheat ahead of the leading shock wave and diffusive effects in the heating zone, and make hydrodynamic stability of LD detonations much different from that of CCD detonations. In this paper, we present experimental results on the hydrodynamic stability of LD detonations propagating in nitrogen and helium gases.

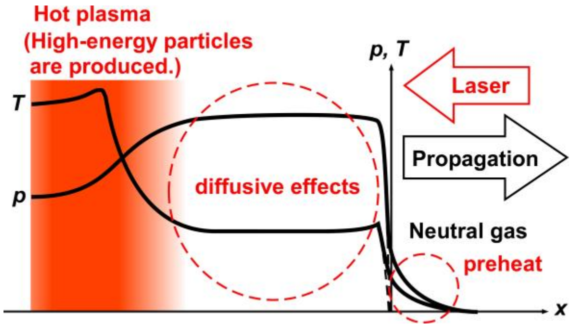


Fig. 2 Schematic of the one-dimensional structure of an LD detonation.

## 2 Experimental arrangement

The experiments were carried out by using the GEKKO XII-HIPER glass laser system [10] at the Institute of Laser Engineering, Osaka University. Figure 3 shows the experimental arrangement. An aluminum target was irradiated by laser in a gas at the temperature of $24(\pm 0.3)$ °C. Flat plates and sinusoidally-corrugated plates were used as targets, the details of which are shown in Fig. 4. The pulse duration of the drive laser was approximately 17.5 ns, and the pulse shape is shown in Fig. 3. The spot diameter of the laser irradiation $d_{spot}$ was 2.3 mm. The energy flux of the drive laser $S_L$ was $1.4\times10^{10}$ W/cm$^2$. For uniform laser irradiation, eleven or twelve laser beams, which were bundled together, were overlapped on the same area of the target surface. The focusing $F$ number of each beam was 16.6, and that of bundled beams was 3.03. Nitrogen and helium gases were used as the media in which LD detonations propagated.

For diagnostics, an optical streak camera (SC) and an optical gate camera (GC) were used. By the SC, a streaked one-dimensional self-emission image, whose width was 100 μm, along the center axis of the bundled laser beams was observed through a 0.532-μm cut filter. The temporal and spatial resolutions of the SC system were approximately 0.66 ns and 30 μm, respectively. By the GC, gated two-dimensional Schlieren images were observed, where the second harmonic of

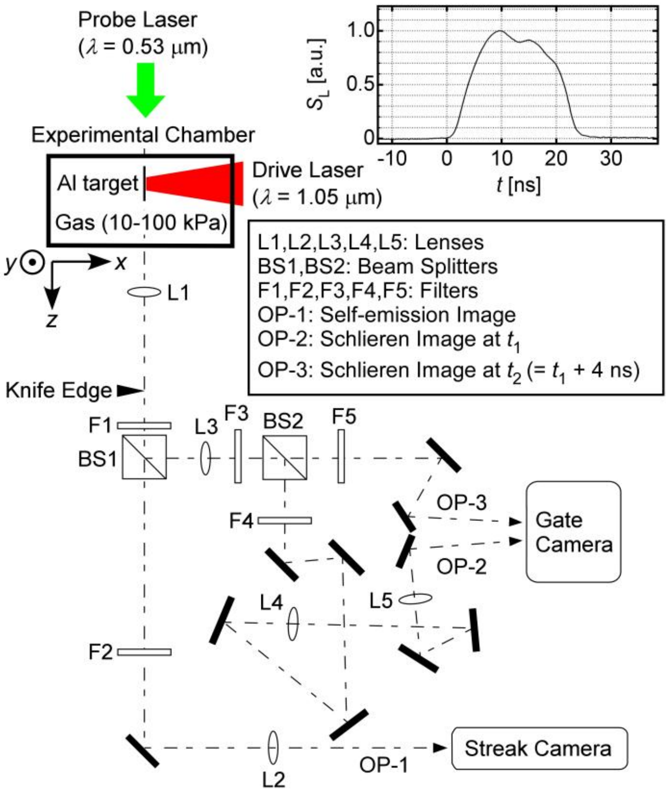


Fig. 3 Experimental arrangement.

a YAG laser and a band-pass filter for 0.532 μm were used. By dividing the optical path to the GC into two and making their path lengths different, two gated images at different times were simultaneously observed. The exposure duration and spatial resolution of the GC system were approximately 200 ps and 60 μm, respectively.

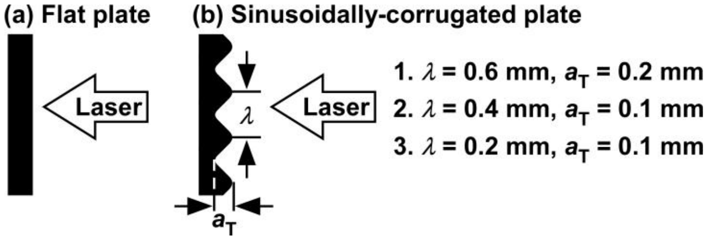


Fig. 4 Details of the targets.

## 3 Results and discussions

First, we show and discuss the results for the cases where nitrogen gas was used as the propagation medium. Figure 5 shows typical results for a flat-plate target, where $p_1$ is the initial gas pressure. Figure 5(a) shows a streaked self-emission image, and Figs. 5(b) and 5(c) show gated Schlieren images. The time $t = 0$ corresponds to the detection limits of the streaked self-emission image and of the laser-pulse waveform shown in Fig. 3. In Fig. 5(d), the exposure profiles of the self emission at three different times and the position of the shock wave, which is the average of those at $t_1$ and $t_2$, are shown, where each exposure profile is normalized so that the peak of each profile is unity, and $x_{50\%}$ is the $x$ coordinate at which the normalized exposure profile is 0.5 in the rising portion. The streaked self-emission image shows that a hot region moved toward positive $x$ direction, where the directions of $x$, $y$, and $z$ axes were defined in Fig. 3. The origin of $y$ coordinate corresponds to the height of the center axis of the bundled drive laser beams, and that of $x$ coordinate corresponds to the initial target surface at $y = 0$. The times $t_1$ and $t_2$ at which the gated images were observed are shown in the corresponding streaked image. The correlation between the times in the SC and GC was determined by observing the same self-emission image by both the SC and GC by using appropriate filters and comparing their spatial profiles. Because the detonation propagated in unconfined gaseous medium, the peripheral border of the front was affected by a rarefaction wave. However, the central portion of the front was quite planar. In order to avoid significant influence of the rarefaction wave on the wave-front structure, we restricted the experimental conditions so that the propagation distance of LD detonations was less than the spot diameter of the laser irradiation.

It should be noted that the leading shock wave shown in Figs. 5(b) and 5(c) are very smooth and no transverse-wave structure was observed. That is, the detonation wave seemed hydrodynamically stable although we can say nothing about finer structure than the spatial resolution of the Schlieren imaging system that was about 60 μm. The data shown in Figs. 5(b) and 5(c) also reveal another interesting feature. In the optical arrangement shown in Fig. 3, the Schlieren image becomes dark when

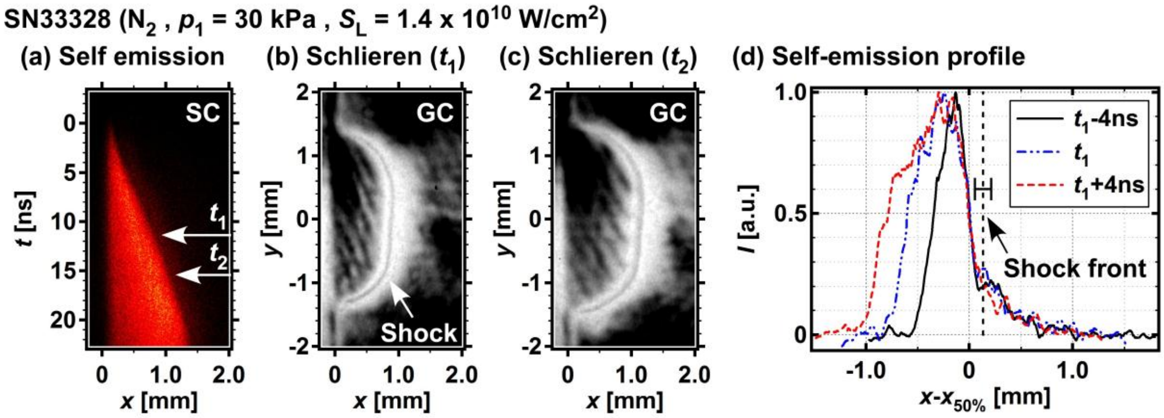


Fig. 5 Typical data for a flat-plate target in nitrogen gas.

$\partial\rho/\partial x < 0$ where $\rho$ is the mass density, and it becomes bright when $\partial n_e/\partial x < 0$. It is remarkable that the region ahead of the leading shock wave is bright as shown Figs. 5(b) and 5(c). This suggests that free electrons existed ahead of the leading shock wave with $\partial n_e/\partial x < 0$. These free electrons were produced by the photoelectric effect by relatively high-energy photons emitted from the hot plasma [11,12]. By these free electrons, the drive laser started to be absorbed via inverse bremsstrahlung before shock heating, and accordingly considerable preheating occurred as shown in Fig. 5(d). Such peculiar heating structure may be relevant to the observed hydrodynamic stability of the LD detonations.

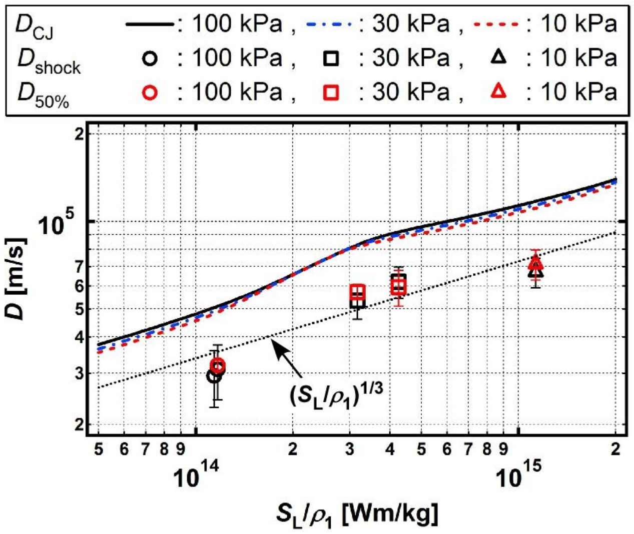


Fig. 6 Detonation propagation speed.

Figure 6 shows the measured speed of shock-wave propagation $D_{shock}$ and that of heating-zone propagation $D_{50\%} = dx_{50\%}/dt$ together with $D_{CJ}$ calculated by the equilibrium calculation and the mass, momentum and energy conservation laws assuming 100% laser absorption. For the equation of state of the plasma, the ion number density $n_z$ for each ionic charge state $z$ was calculated by the Saha equation for given $\rho$ and $T$, where $T$ is the temperature. The electron number density $n_e$ was calculated by the charge neutrality, and the pressure $p$ was calculated by $p = \left(n_e + \sum_z n_z\right) k_B T$, where $k_B$ is the Boltzmann constant. For the caloric equation of state, the energies consumed for dissociation and ionization were all included. When laser is completely absorbed in a detonation wave in steady state, $q_{ext} = S_L/(\rho_1 D_{CJ})$ where $\rho_1$ is the initial mass density of the gas. Further assuming $|q_{react}| \propto q_{ext}$, we can obtain a scaling $D_{CJ} \propto (S_L/\rho_1)^{1/3}$ from eq. (1), and the data can be fitted by this scaling as shown in Fig. 6.

As shown in Fig. 6, $D_{shock}$ and $D_{50\%}$ are in good agreement. In addition, the rising portion of the self-emission profile was almost steady as shown in Fig. 5(d). These suggest that the observed detonation waves were almost in steady state. Further, the measured speeds were well described by the above simple scaling although they were lower than the calculated $D_{CJ}$. The reason why the measured speeds were lower than the calculated $D_{CJ}$ is not understood yet. The plausible reasons are incomplete absorption of the drive laser in the detonation wave as well as energy loss due to electronic and radiative energy transport. For example, in the case shown in Fig. 5, the effective heating energy flux is estimated to be $0.59 \sim 0.63 \times 10^{10}$ W/cm$^2$ by comparing the calculated $D_{CJ}$ with the measured propagation speeds $D_{50\%}$ and $D_{shock}$, although the incident laser energy flux was $1.4 \times 10^{10}$ W/cm$^2$. From the estimated effective heating energy flux, the temperature of the laser-heated plasma is estimated to be $T_{CJ} = 21 \sim 22$ eV, by which the blackbody radiative energy flux is estimated to be $\sigma T_{CJ}{}^4 = 2.0 \sim 2.5 \times 10^{10}$ W/cm$^2$ where $\sigma$ is the Stefan-Boltzmann constant. This means that the emissivity of $0.3 \sim 0.4$ results in the effective heating energy flux of $0.59 \sim 0.63 \times 10^{10}$ W/cm$^2$. This seems highly plausible.

In general, a planar inert shock wave is hydrodynamically stable. Hence, when its front is corrugated, the shape of the shock front shows a damped oscillation [13]. The oscillation occurs due to pressure perturbation in the shocked region induced by the shock-front corrugation, and its damping occurs due to relaxation of the induced pressure perturbation by fluid flow and transport effects in the shocked region. We examined this feature for LD detonations in nitrogen gas. Typical data are shown in Fig. 7. An LD detonation with a sinusoidally-corrugated leading shock front was generated by laser irradiation of a target with a sinusoidally-corrugated surface shown in Figs. 4 and 7(b) in nitrogen gas. The shock front was still corrugated at $t_1$ as shown in Fig. 7(c). However, its corrugation was almost smoothed out at $t_2$ as shown in Fig. 7(d). Figure 8 shows the amplitude of the shock-front corrugation $a_{SF}$ normalized by the amplitude of the target-surface corrugation $a_T$ as a function of the averaged shock-propagation distance $x_{SF}$ normalized by the corrugation wavelength $\lambda$. Compared with the case of inert shock waves in solid density [13], where the shock front became flattened first at $x_{SF}/\lambda = 0.75 \sim 0.8$ and subsequently the phase inversion occurred, the driving force of the oscillation of the shock-front corrugation seems to be suppressed in the case of LD detonations. This suggests that the pressure perturbation in the shocked region induced by the perturbed shock front was more effectively relaxed in the LD detonations than in the inert shock waves. The electronic and radiative energy transport in laser-heated plasmas probably enhanced the relaxation of the pressure perturbation downstream the shock front.

Finally, we show some results on a case where helium gas was used as the propagation medium. Figure 9 shows typical results for a flat-plate target in helium gas. The format of Fig. 9 is similar to Fig. 5 except that the position of the shock wave is not the average of the two different times but at $t_1$. It should be noted that the transverse-wave structure emerged at $t_2$ as shown in Fig. 9(c). The mechanism for such difference in hydrodynamic stability between nitrogen and helium gases is still unknown.

# 4 Conclusions

We examined hydrodynamic stability of laser-driven detonations by using a glass laser at the driving laser energy flux of 1.4x10$^{10}$ W/cm$^2$, using nitrogen and helium gases as the propagation media in the initial pressure range of 10-100 kPa. It

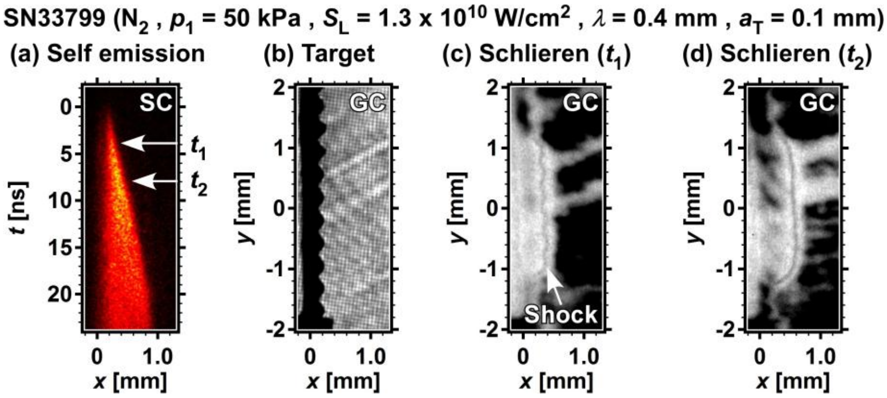


Fig. 7 Typical data on the sinusoidally-corrugated front of an LD detonation in nitrogen gas.

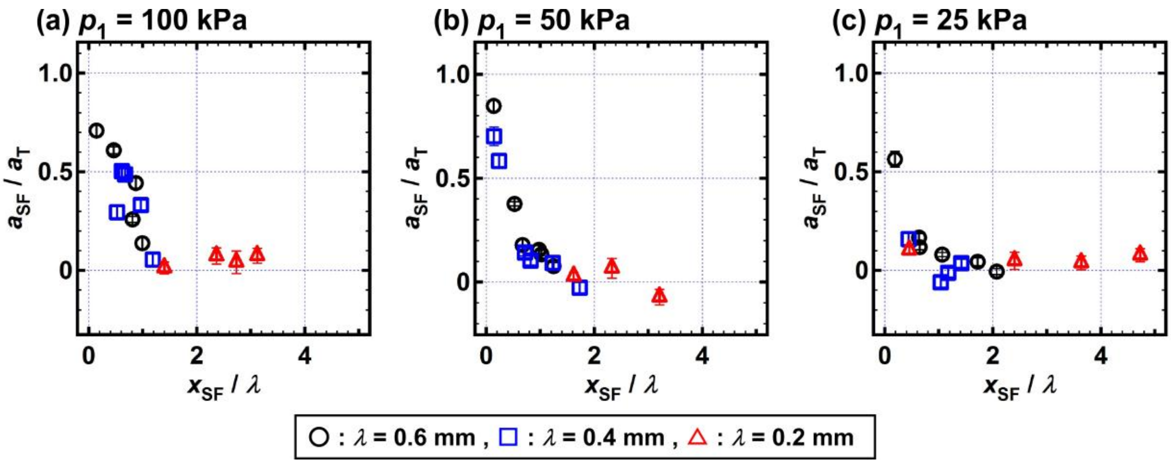


Fig. 8 Amplitude of the shock-front corrugation as a function of shock-propagation distance.

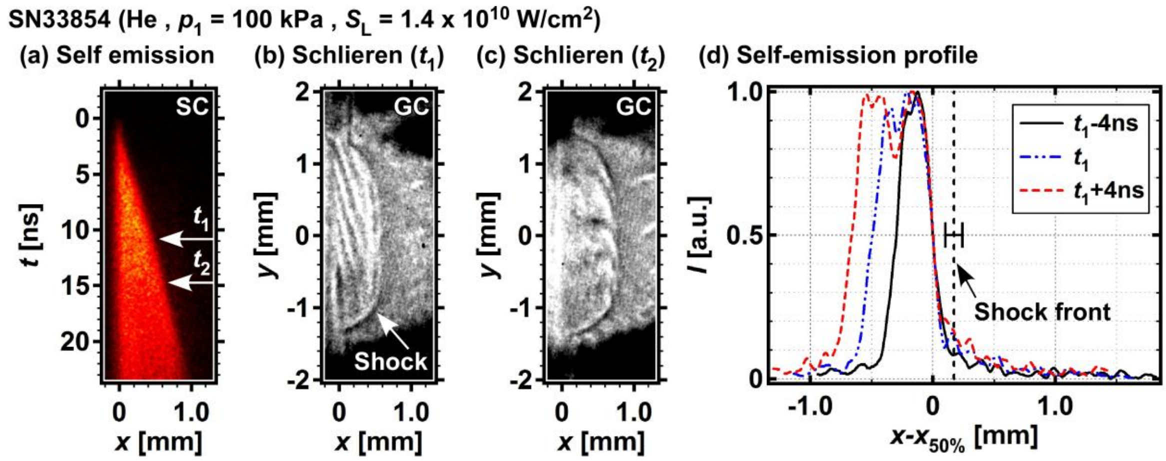


Fig. 9 Typical data for a flat-plate target in helium gas.

was found out that the observed wave front in nitrogen was hydrodynamically stable although the transverse-wave structure was observed in helium.

## Acknowledgment

This work was performed under the auspices of the Collaboration Research Program of the Institute of Laser Engineering, Osaka University.

## References

[1] Fickett W, Davis WC. (1979). Detonation. University of California Press (ISBN 0-520-03587-9).
[2] Lee JHS. (2008). The Detonation Phenomenon. Cambridge University Press (ISBN 978-0-521-89723-5).
[3] Ramsden SA, Savic P. (1964). A Radiative Detonation Model for the Development of a Laser-Induced Spark in Air. Nature 203: 1217.
[4] Raizer YuP. (1965). Heating of a Gas by a Powerful Light Pulse. Sov. Phys. JETP 21: 1009.
[5] Resendes DP, Mota S, Mendonça JT, Sanders B, Encarnação J, del Amo JG, (2007). Laser Propulsion for Ground Launch. J. Propul. Power 23: 73.
[6] Gross RA. (1965). Strong Ionizing Shock Waves. Rev. Mod. Phys. 37: 724.
[7] Boisseau JR, Wheeler JC, Oran ES, Khokhlov AM. (1996). The Multidimensional Structure of Detonations in Type Ia Supernovae. Astrophys. J. 471: L99.
[8] Johzaki T, Nakao Y, Nakashima H, Takabe H, Oda A, Kudo K. (1997). Effects of Neutron Heating on Ignition and Energy Gain of Laser-Imploded D-T Pellets. Laser Part. Beams 15: 259.
[9] Johnston TW, Dawson JM. (1973). Correct Values for High-Frequency Power Absorption by Inverse Bremsstrahlung in Plasmas. Phys. Fluids 16: 722.
[10] Miyanaga N *et al*. (2000). The GEKKO XII-HIPER (High Intensity Plasma Experimental Research) System Relevant to Ignition Targets. 18th IAEA Fusion Energy Conference (Sorrento, Italy, Oct. 2000) Paper No. IAEA-CN-77/IFP/14.
[11] Lin SC. (1962). Radio Echoes from a Manned Satellite during Re-Entry. J. Geophys. Res. 67: 3851.
[12] Wetzel L. (1963). A Feature of Precursor Ionization Profiles due to Shock Radiation. Phys. Fluids. 6: 750; ibid. 6: 1660.
[13] Endo T *et al*. (1995). Dynamic Behavior of Rippled Shock Waves and Subsequently Induced Areal-Density-Perturbation Growth in Laser-Irradiated Foils. Phys. Rev. Lett. 74: 3608; ibid. 75: 2908.